Electrochemistry Communications 115 (2020) 106720

Contents lists available at ScienceDirect

Electrochemistry Communications

journal homepage: www.elsevier.com/locate/elecom

Anodic dissolution of aluminum and anodic passivation in [EMIm]Cl-based ionic liquids

Rene Böttcher*, Adriana Ispas, Andreas Bund

Electrochemistry and Electroplating Group, Department of Electrical Engineering and Information Technology, Technische Universität Ilmenau, Gustav-Kirchhoff-Str. 6, 98693 Ilmenau, Germany

ARTICLE INFO

Keywords:
Aluminum
Ionic liquids
Soluble anode
Anode passivation

ABSTRACT

The anodic dissolution of aluminum in Lewis acidic ionic liquids consisting of $AlCl_3$ and 1-ethyl-3-methylimidazolium chloride was studied using linear sweep and cyclic voltammetry, an electrochemical quartz crystal microbalance (EQCM) and chronopotentiometry at ambient temperature. Anodic passivation of the working electrode was observed in a 2:1 electrolyte while no passivation was found in a 1.5:1 electrolyte. Chronopotentiometry proves the passivation to be caused by local solidification of the electrolyte due to an increase in the aluminum concentration near the anode. EQCM data support these results.

1. Introduction

Electrochemical deposition of aluminum and its alloys is of high interest. Ionic liquids (ILs) have proven to be suitable for this process [1]. Mixtures of $AlCl_3$ and imidazolium-based salts, such as 1-ethyl-3-methylimidazolium chloride, [EMIm]Cl, are intensively studied systems. These electrolytes show good solubility for various metal salts and therefore allow the deposition of aluminum and many of its alloys [2–5]. The Lewis acidity of the melt can be adjusted by varying the molar ratio of [EMIm]Cl and $AlCl_3$, which determines the prevalent anions in the melt (Fig. 1). The melt needs to be Lewis acidic in order to deposit aluminum, according to Eq. (1) [1,6–8]:

$$4Al_2Cl_7^- + 3e^- \rightarrow Al + 7AlCl_4^- \quad (1)$$

Soluble aluminum anodes can be used to achieve a continuous plating process and to avoid anodic decomposition of the IL. However, during the galvanostatic deposition of aluminum from a 2:1 electrolyte the cell voltage increases if soluble aluminum anodes are used at anodic current densities above a critical value of 8.5 mA cm^{-2} at ambient temperature. The deposition process is interrupted once the cell voltage exceeds the compliance of the power supply. This effect can be mitigated within certain limits if high surface area anodes are used, or if the electrolyte is vigorously stirred [9]. However, due to the inhomogeneous distribution of the electrical field there still might be regions on the anode where the local current density exceeds the critical value. This might again lead to the same phenomenon of an increasing cell voltage.

This paper focuses on the dissolution of aluminum in Lewis acidic [EMIm]Cl/$AlCl_3$ ionic liquids with the aim of better understanding the mechanism of anode passivation discussed above. Potentiodynamic polarization experiments as well as cyclic voltammetry measurements are performed to shed light on the limitation of the anodic current density during continuous deposition experiments. A combination of electrochemical quartz crystal microbalance (EQCM) experiments and the application of Sand's theory regarding the concentration profile at the electrode at constant current density [10] is used to explain the increase in the cell voltage at high anodic current densities when a soluble aluminum anode is used.

Controlled current step experiments are powerful methods of studying metal deposition and dissolution characteristics. Depending on the amplitude of the step, the resulting transient gives valuable information about the diffusion coefficient of the electrochemically active species [10,11], the nucleation behavior [6,12] and charge transfer [13].

EQCM is an in situ technique which makes it possible to combine electrochemical measurements with accurate determination of the deposited mass. The decrease in the resonance frequency, Δf, of a quartz crystal is related to the increase in areal mass density, Δm, according to the Sauerbrey equation (Eq. (2)) [14,15]:

$$\Delta f = -\frac{2f_0^2}{(\rho_q \bullet \mu_q)^{1/2}} \bullet \Delta m \quad (2)$$

If one side of the resonator is in contact with a liquid of density ρ_l and viscosity η_l, there is an additional frequency decrease according to

* Corresponding author.
E-mail address: rene.boettcher@tu-ilmenau.de (R. Böttcher).

https://doi.org/10.1016/j.elecom.2020.106720
Received 30 March 2020; Accepted 1 April 2020
Available online 03 April 2020

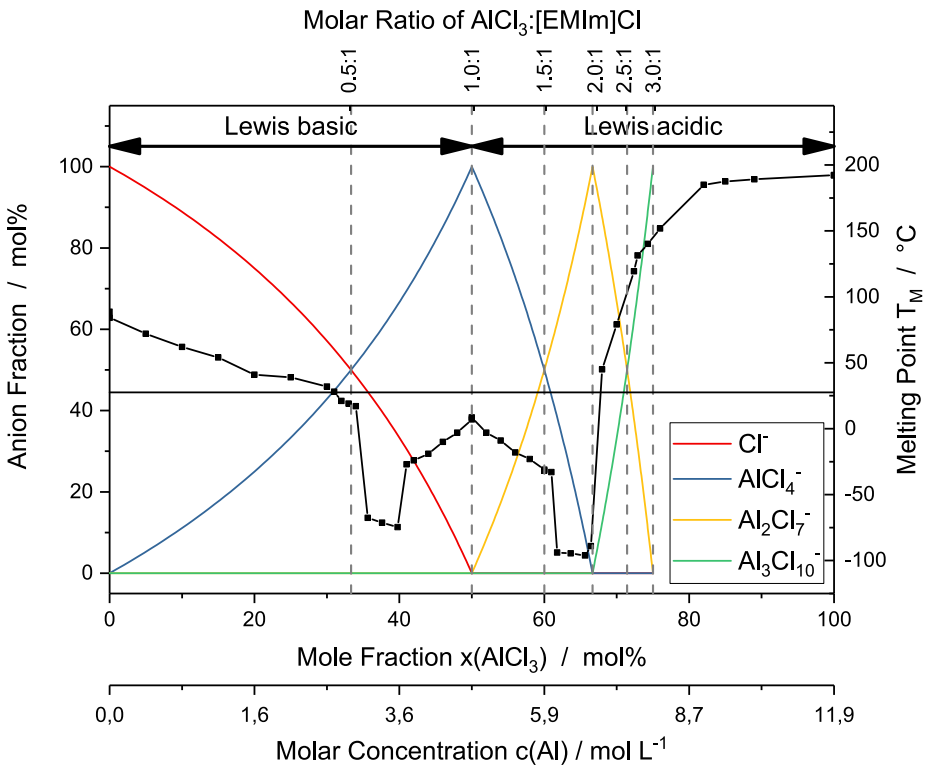

Fig. 1. Theoretical ionic constitution (colored curves) and phase diagram (black line with filled squares) of [EMIm]Cl and $AlCl_3$ [22–24]. The vertical, dashed lines represent the electrolyte composition expressed in molar ratios of $AlCl_3$ to [EMIm]Cl. The horizontal, solid line represents the ambient temperature inside the glovebox. (For interpretation of the references to colour in this figure legend, the reader is referred to the web version of this article.)

the Kanazawa equation (Eq. (3)) [14,16]:

$$\Delta f = -f_0^{3/2} \cdot \left(\frac{\rho_l \cdot \eta_l}{\pi \cdot \rho_q \cdot \mu_q} \right)^{1/2} = -\frac{\Delta w}{2} \tag{3}$$

In Eqs. (2) and (3), f_0 is the resonance frequency of the unloaded quartz, and ρ_q and μ_q are the density and the shear modulus of the quartz, respectively. In order to apply Eq. (2), the change in the damping of the quartz crystal, Δw, should be smaller than the change in the resonance frequency Δf. In our approach, the change in damping of the quartz crystal is measured as the change in the full width at half maximum (FWHM) of the resonance peak of the quartz crystal near its resonance frequency [17]. According to Eq. (3), an increase in the viscosity of the liquid, η_l, in contact with the quartz crystal causes a decrease in frequency and an increase in damping.

2. Experimental

1-Ethyl-3-methylimidazolium chloride, [EMIm]Cl, (> 98%, Iolitec, Germany) was dried at 60 °C for two days to reach a moisture level below 100 ppm (determined by Karl-Fischer titration, model 831 KF Coulometer, Metrohm, Germany [18]). Anhydrous $AlCl_3$ (granules, 99%, abcr, Germany) was used without further purification. The electrolytes were prepared by slow addition of $AlCl_3$ to [EMIm]Cl in molar ratios of 0.5:1 to 2.0:1, which are further denoted as x:1 electrolytes (x = 0.5, 1.0, 1.5, 2.0). Stirring the mixture for 24 h resulted in transparent to slightly yellow liquids depending on the composition.

The electrochemical experiments were performed in an argon-filled glove box (VAC Atmospheres, USA, O_2 < 0.5 ppm, H_2O < 0.5 ppm) using a SP300 or VSP potentiostat/galvanostat (BioLogic, France). For the electrochemical experiments an aluminum wire (99.999%, Alfa Aesar) of 1 mm diameter, sealed in a glass tube with epoxy resin (Epoxy 2000 Plus, Cloeren Technology, Germany), was used as the working electrode (WE). Aluminum plates of 2 mm thickness (99.0%, Goodfellow) were used as ring-shaped counter electrodes (CE). An aluminum wire (99.999%, Alfa Aesar) was used as the reference electrode (RE). In the following all potentials are given with respect to this reference. Before each experiment the WE was sanded with SiC emery paper (800–4000 grit) to prepare an electrode surface of reproducible quality.

Polished AT-cut quartz crystals with a resonance frequency of 10 MHz and gold electrodes of ca. 100 nm thickness (KVG, Germany) were used for the EQCM measurements. The resonance frequency and the damping of the quartz crystal were measured using a network analyzer (Agilent E5100A) while a potentiostat/galvanostat model 263A (EG&G Princeton Applied Research) was used for the electrochemical measurements [19].

3. Results and discussion

From cyclic voltammetry experiments in the potential range −800 mV to +500 mV (scan rate 100 mV s^{-1}) in a 2.0:1 electrolyte (not shown) a coulombic efficiency of > 98% can be calculated, showing the reversibility of the deposition and dissolution of aluminum. Potentiodynamic polarization experiments (Fig. 2(a)) show that the current density decreases strongly at +150 mV and a plateau-like region follows for a 2.0:1 electrolyte (Fig. 2(a)), red curve). This curve shape is characteristic of passivation of the surface. This anodic passivation does not occur in a 1.5:1 electrolyte (Fig. 2(a), black curve), where the equilibrium concentration of Al^{3+} is significantly lower than in a 2.0:1 electrolyte, resulting in a better ability to dissolve aluminum. The passivation potential shifts anodically and the peak current density increases with increasing sweep rate (Fig. 2(a) and (b)). The deposition of aluminum sets in at −80 mV (Fig. 2(b)). The deposited mass increases continuously in the potential range −80 mV to −800 mV. The average slope of the Δm vs. ΔQ plot is (84.3 ± 0.1) µg C^{-1}, which is close to the theoretical value of 93.2 µg C^{-1} for pure aluminum. The lower value probably results from the incorporation of lighter elements (e.g. carbon from $[EMIm]^+$). The exact mass-charge balance of the decomposition of $[EMIm]^+$ is not clear [20,21]. Therefore, an assumption regarding the amount of incorporated impurities cannot be made. The damping of the quartz crystal increases but is significantly lower than the frequency decrease (Fig. 2(b)). Hence Eq. (2) applies. A possible explanation for this slight damping increase is that the

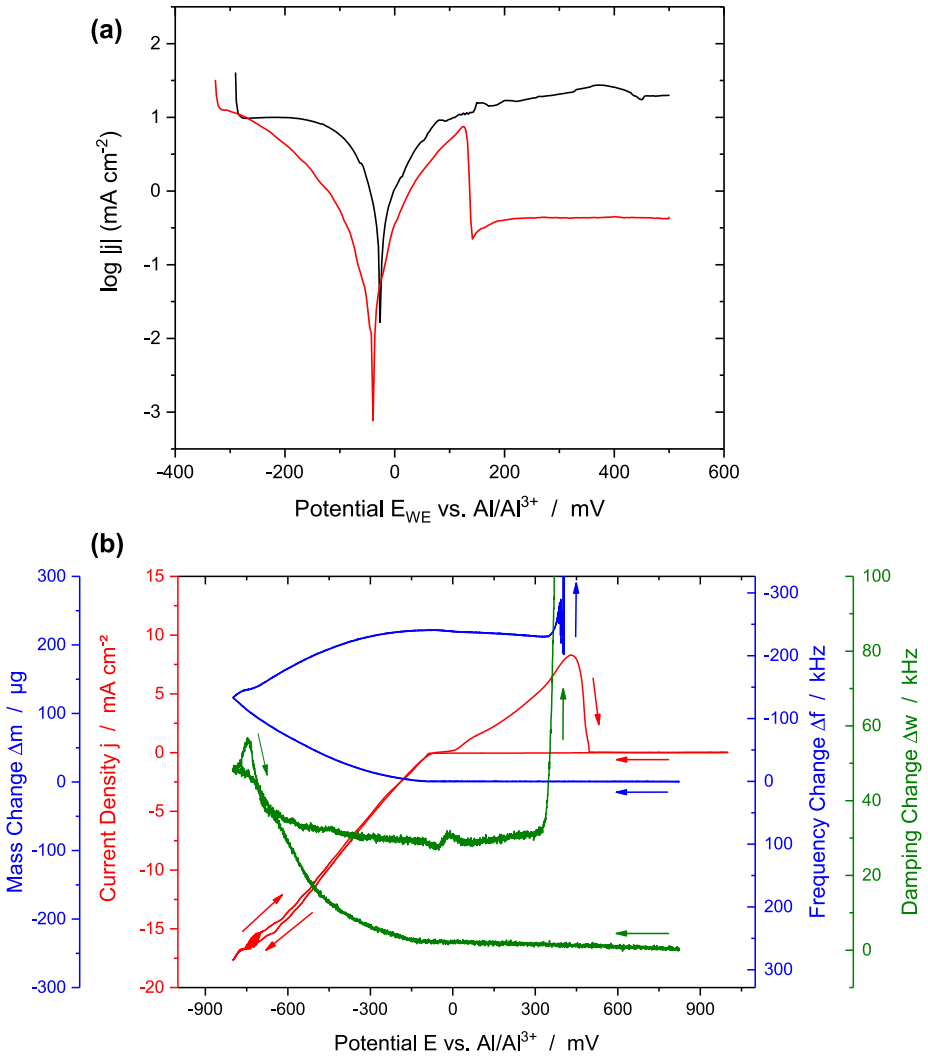

Fig. 2. (a) Potentiodynamic polarization curves of an aluminum electrode in a 1.5:1 (black) and 2.0:1 (red) electrolyte, respectively, (sweep rate 0.1 mV s^{-1}) and (b) cyclic voltammogram and change in frequency, damping and mass in EQCM measurements (sweep rate 1 mV s^{-1}) in a 2.0:1 electrolyte. (For interpretation of the references to colour in this figure legend, the reader is referred to the web version of this article.)

roughness of the deposit is higher than that of the gold layer underneath. Thus the energy is dissipated and the damping increases [15]. Shortly before reaching the vertex potential of −800 mV, the current density oscillates and the damping of the quartz crystal reaches its maximum at around −700 mV on the anodic scan. The depletion in aluminum ion concentration causes the Lewis acidity to decrease and a slight increase in the melting point (Fig. 1), causing higher electrolyte viscosity and hence higher damping. When sweeping the potential anodically, the mass increases further. The average slope of the Δm vs. ΔQ plot in this region was (77.0 ± 0.1) µg C^{-1}. This might indicate electrochemical decomposition of $[EMIm]^+$ and incorporation of the decomposition products of $[EMIm]^+$ formed at more cathodic potentials [20,21]. The change in damping decreases on the anodic scan. Compared to the cathodic scan, the damping remains higher, which is a result of the depletion of the electrolyte, as mentioned above. Liu et al. [20] reported a grain-refining effect of the decomposition products of $[EMIm]^+$. Hence, the deposit has a smoother morphology and roughness effects [15] should then be negligible, leading to a decreasing damping change for the anodic scan, especially just after the vertex potential of −800 mV. An anodic peak current density of 8.5 mA cm^{-2} at 430 mV can be observed, which is in agreement with the potentiodynamic polarization measurements (Fig. 2(a)). At potentials more anodic than 430 mV the current density drops steeply to 35 µA cm^{-2}, indicating passivation. The EQCM indicates a strong frequency decrease and damping increase before the anodic current density drops (Fig. 2(b)). At this point Eq. (2) must be used with caution, since it strictly applies only if the change in damping is smaller than the frequency change. Since there is no cathodic current in this potential range, electrochemical deposition of any material can be excluded. Chlorine evolution would cause a noisy current density transient, which is not observed and can therefore also be excluded. However, the increase in the damping indicates an increase in the viscosity of the electrolyte (Eq. (3)).

The melting point of the electrolyte increases strongly if the molar concentration of $AlCl_3$ exceeds 67 mol% (Fig. 1, molar ratio of 2.0:1). While the melting point of a 2.0:1 electrolyte is around −90 °C, the melting point of a 2.5:1 electrolyte is above 100 °C. Consequently, the increasing cell voltage at high anodic current densities may have its origin in local solidification of the electrolyte due to increasing aluminum concentration at the anode surface. Presumably, the solidifying electrolyte precipitates as a poorly conductive solid and blocks the active electrode surface. Consequently, the local current density at the active anode surface and the potential necessary to drive the charge transfer increase. This results in the passivation of the whole anode surface and is in agreement with the decreasing frequency and increasing damping of the EQCM in the anodic region of the cyclic

voltammogram (Fig. 2(b)). In addition, this explains the shift of the passivation potential with increasing sweep rate. During the cathodic scan, the electrolyte at the electrode surface becomes more Lewis basic. On the anodic scan, aluminum ions still diffuse from the bulk towards the electrode surface when anodic dissolution of aluminum starts. The locally more Lewis-basic electrolyte is able to dissolve more aluminum before exceeding the critical concentration and local solidification occurs. This effect is stronger the higher the sweep rate is, resulting in a shift of the passivation potential towards more anodic values with increasing sweep rate.

If the origin of the passivation phenomenon described above is the solidification of the electrolyte due to increased aluminum concentration in front of the anode, it is mainly caused by slow diffusion. Consequently, current step experiments are suitable to support this theory. The diffusion coefficient of $Al_2Cl_7^-$ ions was found to be $(7.1 \pm 0.3)\cdot10^{-11}$ m^2 s^{-1}, evaluated from controlled current and potential step experiments (not shown). The critical aluminum concentration at which the electrolyte solidifies for a given temperature can be evaluated from the phase diagram of $AlCl_3$ and [EMIm]Cl (Fig. 1). For this calculation the abscissa in Fig. 1 was transformed from mole fraction, $x(AlCl_3)$, to molar concentration, c(Al), using Eqs. (4) and (5):

$$c(\mathrm{Al}) = \frac{\frac{n_{AlCl_3}}{n_{[EMIm]Cl}} \cdot \rho_{IL}}{\frac{n_{AlCl_3}}{n_{[EMIm]Cl}} \cdot M_{AlCl_3} + M_{[EMIm]Cl}} \tag{4}$$

$$\frac{n_{AlCl_3}}{n_{[EMIm]Cl}} = \frac{x(AlCl_3)}{1 - x(AlCl_3)} \tag{5}$$

The critical mole fraction, $x_{crit}(AlCl_3)$, was calculated by interpolation of the respective points from Fig. 1 that intercept a temperature of 27.5 °C at an aluminum concentration above that for a 2.0:1 electrolyte. This concentration ($x_{crit}(AlCl_3)$ = 68.85 mol%) equals c_{crit} = 7.24 mol L^{-1}.

Fig. 3 shows the theoretical concentration profiles of a 2.0:1 electrolyte in front of an aluminum anode with different applied current densities and times. The plot is based on the Sand equation, which describes the concentration profile at an electrode [10] (Eq. (6)):

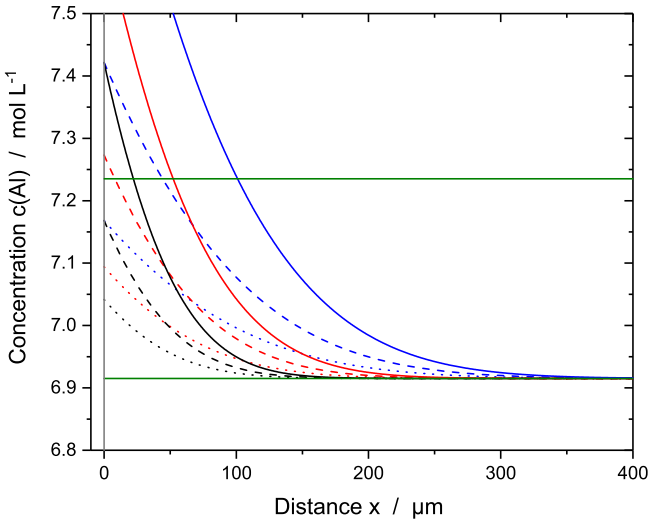

Fig. 3. Concentration profile $c(x,t)$ of a 2.0:1 electrolyte near an aluminum electrode with an applied anodic current density j of 5 mA cm^{-2} (dotted lines), 10 mA cm^{-2} (dashed lines) and 20 mA cm^{-2} (solid lines) depending on the dissolution time t of 30 s (black), 60 s (red) and 120 s (blue), based on Eq. (6) [10] and using a diffusion coefficient of $(7.1 \pm 0.3)\cdot10^{-11}$ m^2 s^{-1}. The solid horizontal lines represent c_{crit} (upper line) and c^* (lower line) for 27.5 °C, respectively. (For interpretation of the references to colour in this figure legend, the reader is referred to the web version of this article.)

$$c(x,t) = c^* - \frac{j}{zFD} \cdot \left(\left(\frac{4tD}{\pi} \right)^{1/2} \cdot \exp\left(-\frac{x^2}{4tD} \right) - x \cdot erfc\left(\frac{1}{(4tD)^{1/2}} \right) \right) \tag{6}$$

In Eq. (6) c is the concentration, x is the distance from the electrode, t is the time after application of the current step, c^* is the bulk concentration of the electrolyte, j is the applied current density, z is the number of exchanged electrons, F is the Faraday constant and D is the diffusion coefficient. The concentration of aluminum ions near the electrode increases rapidly when a constant current density is applied. For a low current density (e.g. 5 mA cm^{-2}) the critical concentration c_{crit} is not reached within a time frame of some minutes (2 min for 5 mA cm^{-2}). For higher current densities (e.g. 10 or 20 mA cm^{-2}) the concentration exceeds the limit in less than one minute and natural convection will not have a strong impact on the concentration profile. A refined theory would have to take into consideration enhanced mass transport due to natural convection, influencing the concentration profile.

The critical transition time, τ_{crit}, can be defined as the time it takes for the concentration at the electrode surface (x = 0) to reach the critical concentration, c_{crit}. It can be expressed according to Eq. (7), based on Eq. (6):

$$\tau_{crit} = (c_{crit} - c^*)^2 \cdot \frac{(zF)^2 \cdot D\pi}{4j^2} \tag{7}$$

Fig. 4(a) shows the calculated critical transition times depending on the applied current density and measured transition times from a 2.0:1 electrolyte. Despite a minor deviation from the theoretical curves, the measured values of τ_{crit} are in good agreement with the discussed model. Over the whole region of current densities, the measured values are between the theoretical ones for 2.0:1 and 1.9:1 electrolytes. Slightly higher critical transition times might be the result of a slightly delayed onset of the nucleation of the solidifying melt (supercooling) as can also be deduced from the EQCM measurements, showing the damping to increase before the frequency decreases, accompanied by the decrease in the current density (Fig. 2(b)). Furthermore, one should keep in mind that Eq. (6) only applies for semi-infinite diffusion. The theoretical values in Fig. 4 are based on fitting the density for different electrolyte compositions and the diffusion coefficients from high amplitude potential and current step experiments (not shown). Furthermore, the difference in the mass of $AlCl_3$ for the preparation of a 2.0:1 and 1.9:1 is about 2.0 to 2.5%. Hence, a deviation between theoretical and experimental data results from errors in the mass (accuracy of the balance used is 1 mg) for the preparation of the melt. The interpolation of the data for the melting point when evaluating the critical concentration might also lead to deviations. Only two points of the phase diagram (Fig. 1) are taken into account. The difference in aluminum concentration between these is about 1.6 mol%. Hence, the necessary effort to prepare electrolytes of different composition between these two is quite high. However, the results are in a reasonable range, taking into account the errors caused by these factors.

The plot of the current density vs. the inverse square root of the critical transition time shows linear behavior and a zero intercept (Fig. 4(b)), indicating diffusion control. Consequently, the passivation of the anode is caused by low diffusion of aluminum ions from the anode into the electrolyte, local solidification of the electrolyte due to the increased aluminum concentration and its precipitation on the anode. Comparable effects were reported for high temperature molten salts [25,26]. Since the melting temperature increases steeply within a small concentration range up to approximately 130 °C (Fig. 1), increasing the temperature improves the anodic dissolution of aluminum into the electrolyte only slightly. Even at elevated temperatures the dissolution of aluminum in a 2.0:1 electrolyte will be limited by the ability of the electrolyte to dissolve aluminum before exceeding the local solidification point. Furthermore, the thermal decomposition of $[EMIm]^+$ is also a limiting factor. The solubility of various metal salts in this type of IL increases with the Lewis acidity of the electrolyte [1]

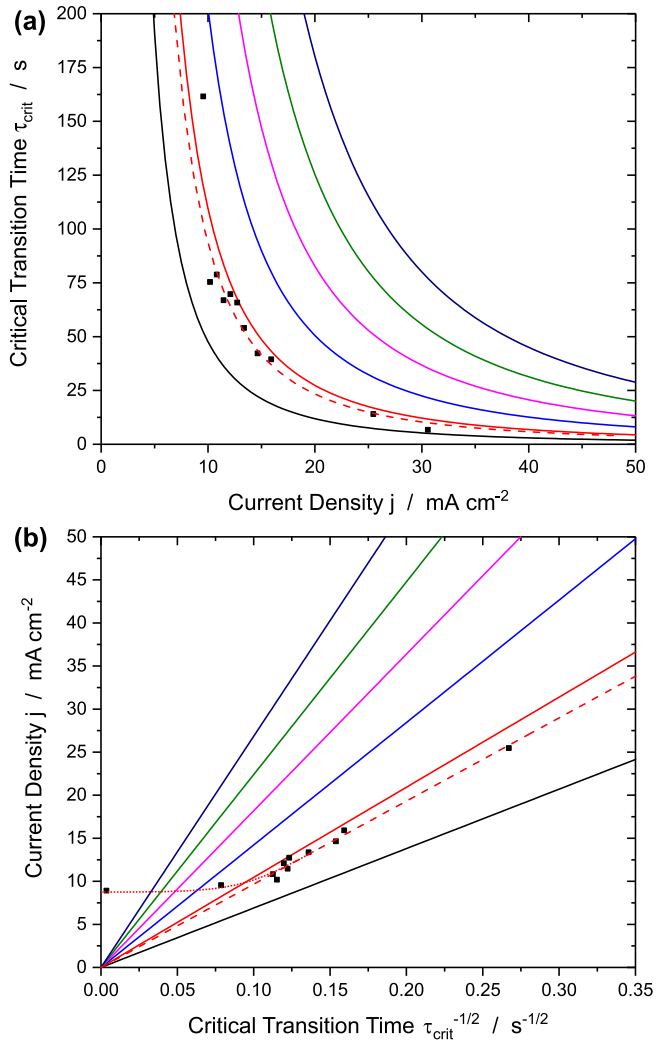

Fig. 4. (a) Critical transition time τ_{crit} and (b) its inverse square root vs. the current density *j* for 2.0:1 (black), 1.9:1 (red), 1.8:1 (blue), 1.7:1 (violet), 1.6:1 (green) and 1.5:1 (dark blue) electrolytes. The experimental critical transition times (black dots), the linear fit for $\tau_{crit} < 1$ min (red dotted line) and the trend line (red dashed line) are also shown. (For interpretation of the references to colour in this figure legend, the reader is referred to the web version of this article.)

which is an important consideration for the deposition of aluminum alloys. Consequently, a compromise between Lewis acidity and the tendency of the electrolyte to cause anodic passivation has to be found. Furthermore, the addition of metal salts other than aluminum chloride to this type of electrolyte might also cause a change in the melting point [27,28]. The impact of this has to be taken into account for each individual electrolyte.

For small current densities the experimental critical transition times deviate from the theoretical values, which can be explained by the onset of natural convection. For the system investigated here, an approximate critical anodic current density of 8.5 mA cm^{-2} at (27.5 ± 2.5) °C can be estimated for a 2.0:1 electrolyte (Fig. 4(b)). This value represents the maximum applicable current density to avoid transport limitations and hence the passivation of the anode for stationary deposition conditions. Therefore, it can be found in the potentiodynamic polarization curve of a 2.0:1 electrolyte (Fig. 2(a)) and in the EQCM coupled cyclic voltammogram (Fig. 2(b)).

4. Conclusions

While electrolyte anodic passivation occurs in a 2.0:1 [EMIm]Cl-$AlCl_3$, no passivation is observed in a 1.5:1 electrolyte. The EQCM indicates a frequency decrease and damping increase immediately before the current density drops due to passivation, indicating solidification and precipitation of the electrolyte on the electrode.

Controlled-current step experiments showed mass transport to be limiting for the anodic dissolution of aluminum at high current densities. A high dissolution rate of aluminum causes a strong increase in the melting point of the electrolyte, which then solidifies and precipitates on the electrode, causing a passivation due to the formation of a poorly conductive film, in accordance with the EQCM measurements. For electrolytes with a low aluminum concentration, intense stirring or a high ratio of anode to cathode area are recommended for long-term deposition processes to prevent anodic passivation.

The results can be transferred to other electrolytes that show eutectic behavior combined with slow diffusion and a significant change in viscosity depending on electrolyte composition.

Declaration of Competing Interest

The authors declare that they have no known competing financial interests or personal relationships that could have appeared to influence the work reported in this paper.

Acknowledgements

The authors gratefully acknowledge the financial support of the Federal Ministry of Economic Affairs and Energy (Bundesministerium für Wirtschaft und Energie), within the project NiCO (ref. no. 20W1523H), and support for the Article Processing Charge by the German Research Foundation (DFG) and the Open Access Publication Fund of the Technische Universität Ilmenau. Thanks also go to Mohammadshahabaldin Najafi for his assistance with the electrochemical measurements.

References

[1] F. Endres, A. Abbott, D. Mac Farlane, Electrodeposition From Ionic Liquids, second ed., Wiley-VCH, Weinheim, 2017.
[2] G.R. Stafford, C.L. Hussey, Electrodeposition of transition metal-aluminum alloys from chloroaluminate molten salts, in: R.C. Alkire, D.M. Kolb (Eds.), Adv. Electrochem. Sci. Eng. 7, Wiley-VCH, Weinheim, 2002, pp. 275–348.
[3] Q.X. Liu, S.Z. El Abedin, F. Endres, Electroplating of mild steel by aluminium in a first generation ionic liquid: a green alternative to commercial Al-plating in organic solvents, Surf. Coat. Tech. 201 (2006) 1352–1356.
[4] L. Simanavičius, A. Staknas, A. Šarkis, Codeposition of aluminum with some metals from AlBr 3-dimethylethylphenylammonium bromide solutions containing acetylacetonate of selected metal, Electrochim. Acta 46 (2000) 499–507.
[5] A. Ispas, E. Wolff, A. Bund, An electrochemical quartz crystal microbalance study on electrodeposition of aluminum and aluminum-manganese alloys, J. Electrochem. Soc. 164 (2017) H5263–H5270.
[6] T. Jiang, M.C. Brym, G. Dubé, A. Lasia, G.M. Brisard, Electrodeposition of aluminium from ionic liquids: Part I—electrodeposition and surface morphology of aluminium from aluminium chloride ($AlCl_3$)-1-ethyl-3-methylimidazolium chloride ([EMIm] Cl) ionic liquids, Surf. Coat. Tech. 201 (2006) 1–9.
[7] A. Bakkar, V. Neubert, Electrodeposition and corrosion characterisation of micro- and nano-crystalline aluminium from $AlCl_3$/1-ethyl-3-methylimidazolium chloride ionic liquid, Electrochim. Acta 103 (2013) 211–218.
[8] H.M.A. Abood, N.L. Dawood, Morphology of electrodeposited aluminium metal from aluminium chloride-urea room temperature ionic liquid (RTIL) at variable parameters, Int. J. Sci. Res. (2015) 753–760.
[9] C. Wang, A. Creuziger, G. Stafford, C.L. Hussey, Anodic dissolution of aluminum in the aluminum chloride-1-ethyl-3-methylimidazolium chloride ionic liquid, J. Electrochem. Soc. 163 (2016) H1186–H1194.
[10] H.J.S. Sand III, On the concentration at the electrodes in a solution, with special reference to the liberation of hydrogen by electrolysis of a mixture of copper sulphate and sulphuric acid, Lond. Edinb. Dublin Philos. Mag. J. Sci. 1 (1901) 45–79.
[11] F.G. Cottrell, Der Reststrom bei galvanischer Polarisation, betrachtet als ein Diffusionsproblem, J. Phys. Chem. 42U (1903) 386–431.
[12] V.A. Isaev, Y.P. Zaykov, O.V. Grishenkova, A.V. Kosov, O.L. Semerikova, Analysis of potentiostatic current transients for multiple nucleation with diffusion and kinetic

controlled growth, J. Electrochem. Soc. 166 (2019) D851–D856.
[13] W. Lorenz, Oszillographische Überspannungsmessungen. I, Ber. Bunsenges, Phys. Chem. 58 (1954) 912–918.
[14] V.M. Mecea, From quartz crystal microbalance to fundamental principles of mass measurements, Anal. Lett. 38 (2005) 753–767.
[15] E.M. Moustafa, S.Z. El Abedin, A. Shkurankov, E. Zschippang, A.Y. Saad, A. Bund, F. Endres, Electrodeposition of Al in 1-butyl-1-methylpyrrolidinium bis(trifluoromethylsulfonyl)amide and 1-ethyl-3-methylimidazolium bis(trifluoromethylsulfonyl)amide ionic liquids, J. Phys. Chem. B 111 (2007) 4693–4704.
[16] K.K. Kanazawa, J.G. Gordon, The oscillation frequency of a quartz resonator in contact with liquid, Anal. Chim. Acta 175 (1985) 99–105.
[17] A. Ispas, A. Bund, F. Endres, Application of the electrochemical quartz crystal microbalance for the investigation of metal depositions from ionic liquids, ECS Trans. 16 (2009) 411–420.
[18] M. Stich, N. Pandey, A. Bund, Drying and moisture resorption behaviour of various electrode materials and separators for lithium-ion batteries, J. Power Sources 364 (2017) 84–91.
[19] A. Ispas, B. Adolphi, A. Bund, F. Endres, On the electrodeposition of tantalum from three different ionic liquids with the bis(trifluoromethyl sulfonyl) amide anion, Phys. Chem. Chem. Phys. 12 (2010) 1793–1803.
[20] Q.X. Liu, S.Z. El Abedin, F. Endres, Electrodeposition of nanocrystalline aluminum, J. Electrochem. Soc. 155 (2008) D357–D362.
[21] J. Tang, K. Azumi, Optimization of pulsed electrodeposition of aluminum from AlCl 3-1-ethyl-3-methylimidazolium chloride ionic liquid, Electrochim. Acta 56 (2011) 1130–1137.
[22] A.A. Fannin Jr, D.A. Floreani, L.A. King, J.S. Landers, B.J. Piersma, D.J. Stech, R.L. Vaughn, J.S. Wilkes, J.L. Williams, Properties of 1, 3-dialkylimidazolium chloride-aluminum chloride ionic liquids, J. Phys. Chem. 88 (1984) 2614–2621.
[23] M. Zhang, R. Groves, R.M. Counce, J.S. Watson, T.A. Zawodzinski, Melting/freezing points of high concentrations of $AlCl_3$ in a saturated chloroaluminate ionic liquid, J. Therm. Anal. Calorim. 124 (2016) 395–398.
[24] H.A. Øye, M. Jagtoyen, T. Oksefjell, J.S. Wilkes, Vapour pressure and thermodynamics of the system 1-methyl-3-ethyl-imidazolium chloride – aluminium chloride, MSF 73–75 (1991) 183–190.
[25] G.L. Holleck, J. Giner, The aluminum electrode in $AlCl_3$-alkali-halide melts, J. Electrochem. Soc. 119 (1972) 1161–1166.
[26] D. Orbakh, Nonaqueous Electrochemistry, first ed., Marcel Dekker, New York, 1999.
[27] W.R. Pitner, Electrodeposition of zinc from the Lewis acidic aluminum chloride-1-methyl-3-ethylimidazolium chloride room temperature molten salt, J. Electrochem. Soc. 144 (1997) 3095–3103.
[28] S.-I. Hsiu, J.-F. Huang, I.-W. Sun, Ch.-H. Yuan, J. Shiea, Lewis acidity dependency of the electrochemical window of zinc chloride–1-ethyl-3-methylimidazolium chloride ionic liquids, Electrochim. Acta 47 (2002) 4367–4372.